Inorg. Chem. **2005**, *44*, 6967−6974

A 2D Layered Spin Crossover Complex Constructed by NH···Cl^- Hydrogen Bonds: $[Fe^{II}H_3L^{Me}]Cl\cdot I_3$ (H_3L^{Me} = Tris[2-(((2-methylimidazoyl-4-yl)methylidene)amino)ethyl]amine

Masahiro Yamada,[†] Eri Fukumoto,[†] Makoto Ooidemizu,[†] Nicolas Bréfuel,[†] Naohide Matsumoto,*[,†] Seiichiro Iijima,[‡] Masaaki Kojima,[§] Nazzareno Re,[||] Françoise Dahan,[⊥] and Jean-Pierre Tuchagues[⊥]

Department of Chemistry, Faculty of Science, Kumamoto University, Kurokami 2-39-1, Kumamoto 860-8555, Japan, National Institute of Advanced Industrial Science and Technology, Tsukuba 305-8566, Japan, Department of Chemistry, Faculty of Science, Okayama University, Tsushima-naka 3-1-1, Okayama 700-8530, Japan, Facolta di Farmacia, Università degli Studi "G. D'Annunzio", I-66100 Chieti, Italy, and Laboratoire de Chimie de Coordination du CNRS, UP 8241, 205 Route de Narbonne, 31077 Toulouse Cedex, France

Received January 4, 2005

A 2D layered spin crossover complex, $[Fe^{II}H_3L^{Me}]Cl\cdot I_3$, has been synthesized from the reaction of $Fe^{III}Cl_3$, a tripod ligand (H_3L^{Me} = tris[2-(((2-methylimidazoyl-4-yl)methylidene)amino)ethyl]amine), and NaI in methanol. The compound showed an abrupt spin transition between the HS ($S = 2$) and LS ($S = 0$) states at $T_{1/2} = 110$ K without hysteresis. The crystal structures of the HS and LS states were determined at 180 and 90 K. A 2D layered structure is composed of NH···Cl^- hydrogen bonds between the Cl^- ion and three neighboring imidazole groups of $[Fe^{II}H_3L^{Me}]^{2+}$. The green light irradiation at 5 K induced the LIESST effect, and the thermal relaxation process from the HS to LS state showed a sigmoid curve at $T > 55$ K.

Introduction

The spin crossover (SC) compounds are one of the representative examples of molecular bistability.[1] The high-spin (HS) and low-spin (LS) states of an SC compound are interconvertible by several different physical perturbations such as temperature, pressure, and light irradiation.[1,2] While SC behavior is essentially a phenomenon of a single molecule, the interaction between SC sites is an important factor to govern SC properties such as the abruptness of the spin transition, hysteresis, and LIESST (light-induced excited spin state trapping) effect, which are important properties for applications such as information storage, molecular switches, and visual displays.[3] From this viewpoint, the synthetic design of SC compounds exhibiting interactions between spin-transition sites is of current interest. Along this line, polymeric SC compounds with bridging ligands[4] and mononuclear SC compounds exhibiting intermolecular interactions such as hydrogen bonding and $\pi-\pi$ stacking[5] have been extensively investigated. Previously, we reported a family of 2D SC complexes, $[Fe^{II}H_3L^{Me}][Fe^{II}L^{Me}]X$ (H_3L^{Me} =tris[2-(((2-methylimidazoyl-4-yl)methylidene)amino)ethyl]-amine, X = NO_3^-, ClO_4^-, BF_4^-, PF_6^-, AsF_6^-, SbF_6^-), in which two component Fe^{II} sites, $[Fe^{II}H_3L^{Me}]^{2+}$ and $[Fe^{II}L^{Me}]^-$,

* To whom correspondence should be addressed. E-mail: naohide@aster.sci.kumamoto-u.ac.jp. Fax: +81-96-342-3390.
[†] Kumamoto University.
[‡] National Institute of Advanced Industrial Science and Technology.
[§] Okayama University.
[||] Università degli Studi "G. D'Annunzio".
[⊥] Laboratoire de Chimie de Coordination du CNRS Toulouse.

(1) (a) König, E. *Prog. Inorg. Chem.* **1987**, *35*, 527−623. (b) Goodwin, H. A. *Coord. Chem. Rev.* **1976**, *18*, 293−325. (c) Gütlich, P.; Hauser, A.; Spiering, H. *Angew. Chem., Int. Ed. Engl.* **1994**, *33*, 2024−2054. (d) Gütlich, P.; Goodwin, H. A. *Spin Crossover in Transition Metal Compounds I*−*III*; Topics in Current Chemistry, 233−235; Springer: New York, 2004.
(2) (a) Decurtins, S.; Gütlich, P.; Köhler, C. P.; Spiering, H.; Hauser, A. *Chem. Phys. Lett.* **1984**, *105*, 1−4. (b) Gütlich, P.; Garcia, Y.; Woike, T. *Coord. Chem. Rev.* **2001**, *219*−221, 839−879. (c) Hauser, A. *J. Chem. Phys.* **1991**, *94*, 2741−2748.
(3) (a) Kahn, O.; Martinez, J. C. *Science* **1998**, *279*, 44−48. (b) van Koningsbruggen, P. J.; Garcia, Y.; Kahn, O.; Fournes, L.; Kooijman, H.; Spek, A. L.; Haasnoot, J. G..; Moscovici, J.; Provost, K.; Michalowicz, A.; Renz, F.; Gütlich, P. *Inorg. Chem.* **2000**, *39*, 1891−1900. (c) Real, J. A.; Andres, E.; Munoz, M. C.; Julve, M.; Granier, T.; Bousseksou, A.; Varret, F. *Science* **1995**, *268*, 265−267.
(4) (a) Garcia, Y.; Kahn, O.; Rabardel, L.; Chansou, B.; Salmon, L.; Tuchagues, J.-P. *Inorg. Chem.* **1999**, *38*, 4663−4670. (b) Breuning, E.; Ruben, M.; Lehn, J.-M.; Renz, F.; Garcia, Y.; Ksenofontov, V.; Gütlich, P.; Wegelius, E.; Rissanen, K. *Angew. Chem., Int. Ed.* **2000**, *39*, 2504−2507. (c) Moliner, N.; Munoz, C.; Letard, S.; Solans, X.; Menendez, N.; Goujon, A.; Varret, F.; Real, J. A. *Inorg. Chem.* **2000**, *39*, 5390−5393.

10.1021/ic050008f CCC: $30.25
Published on Web 08/30/2005

are connected through an imidazole−imidazolate hydrogen bond to produce a 2D extended network structure.[6] Due to the network structure constructed by the imidazole−imidazolate hydrogen bonds (NH···N), the compounds showed a rather abrupt spin transition. These compounds were found to exhibit LIESST effect. During the course of our studies on a family of SC complexes with the same tripod ligand, we found a new type of SC complex with the chemical formula $[Fe^{II}H_3L^{Me}]Cl\cdot I_3$ (**2**). This compound shows an abrupt spin transition, and the crystal structure consists of a new type of 2D extended structure constructed by NH···Cl^- hydrogen bonds. In this paper, we report the synthesis of this new complex, the details of its 2D layer structure, the abrupt spin-transition behavior, and the LIESST effect.

Results and Discussion

Synthesis and Characterization of $[Fe^{II}H_3L^{Me}]I_2\cdot H_2O\cdot$MeOH (1) and $[Fe^{II}H_3L^{Me}]Cl\cdot I_3$ (2). The $[Fe^{II}H_3L^{Me}]I_2\cdot H_2O\cdot$MeOH (**1**) complex was obtained as orange crystals from the mixed solution of the tripod ligand H_3L^{Me}, $Fe^{II}Cl_2\cdot 4H_2O$, and NaI with the molar ratio of 1:1:2 in methanol in the open atmosphere. The $[Fe^{II}H_3L^{Me}]Cl\cdot I_3$ (**2**) complex was synthesized by either method A or method B. Method A: The reaction of the ligand H_3L^{Me}, $Fe^{II}Cl_2\cdot 4H_2O$, and NaI with the molar ratio of 1:1:3 in methanol under acidic conditions (ca. pH = 5) in air produced a mixture of **1** and **2**. A part of I^- is oxidized to I_3^- ($3I^- \rightarrow I_3^- + 2e^-$) by molecular oxygen to yield **2**. Method B: Complex **2** is obtained as pure red crystals from the reaction of H_3L^{Me}, $Fe^{III}Cl_3$, and NaI in methanol. To a solution of the neutral tripod ligand H_3L^{Me} was added a methanolic solution of $Fe^{III}Cl_3$ and then a solution of NaI. The resulting mixture was allowed to stand for several days during which time well-grown red crystals of **2** precipitated. Both Fe^{III} ion and molecular oxygen can oxidize I^- to I_3^- yielding exclusively compound **2**. Methanol also serves as a reducing agent for the Fe^{III} ion ($Fe^{III} + e^- \rightarrow Fe^{II}$).[6]

The infrared (IR) spectra of complexes **1** and **2** showed characteristic bands at 1640 and 1644 cm^{-1}, respectively. The sharp band is assigned to the C═N stretching vibration of the Schiff-base ligand. On the basis of the wavenumber, the HS Fe^{II} state is expected for both complexes.[6]

Table 1. Crystallographic Data for $[Fe^{II}H_3L^{Me}]Cl\cdot I_3$ (**2**)

param	180 K	90 K
formula	$C_{21}H_{30}ClFeI_3N_{10}$	$C_{21}H_{30}ClFeI_3N_{10}$
fw	894.55	894.55
cryst system	monoclinic	monoclinic
space group	$P2_1/c$ (No. 14)	$P2_1/c$ (No. 14)
a, Å	14.0532(16)	13.8092(13)
b, Å	13.0076(9)	12.9422(10)
c, Å	17.2046(18)	16.9409(14)
β, deg	90.035(13)	90.026(11)
V, Å^3	3145.0(5)	3027.7(4)
Z	4	4
F(000)	1712	1712
λ, Å	0.710 73	0.710 73
T, K	180 ± 2	90 ± 2
D_{calc}, Mg m^{-3}	1.889	1.962
μ(Mo Kα), mm^{-1}	3.538	3.675
θ range, deg min−max	2.13−26.04	3.23−32.37
no. of data collcd	24 770	16 357
no. of unique data	6112	8082
R(int)	0.0444	0.0388
no. of variable params	329	329
no. of obsd reflcns[a]	5683	6688
R[b] obsd, all	0.0342, 0.0376	0.0362, 0.0367
wR[c] obsd, all	0.0673, 0.0700	0.0440, 0.0481
S	1.038	1.425
$(\Delta/\sigma)_{max}$	0.000	0.002
$(\Delta/\rho)_{max,min}$, e Å^{-3}	0.889, −1.090	1.030, −0.892

[a] Data with $F_o > 4\sigma(F_o)$. [b] $R = \sum||F_o| - |F_c||/\sum|F_o|$. [c] $wR = [\sum w(|F_o^2| - |F_c^2|)^2/\sum w|F_o^2|^2]^{1/2}$.

Crystal Structure of $[Fe^{II}H_3L^{Me}]Cl\cdot I_3$ (2). Since compound **2** exhibited a spin crossover between the HS ($S = 2$) and LS ($S = 0$) states as demonstrated by the magnetic susceptibility measurements to be described later, the X-ray diffraction data were collected at 180 and 90 K to elucidate the HS and LS structures, where the lowest temperature of the cooling equipment of our X-ray diffractometer is 90 K. To avoid the damage of the crystal at low temperature, the crystal was cooled gradually. The crystallographic data at 180 and 90 K are given in Table 1. The space group is retained in both states. The unit cell volume of 3145.0(5) Å^3 at 180 K is reduced to 3027.7(4) Å^3 at 90 K (3.7% reduction). The volume reduction of 3.7% is substantially smaller than 7.6% of $[Fe^{II}H_3L^{Me}][Fe^{II}L^{Me}]PF_6$ with the NH···N hydrogen bond.[6c] Selected bond distances, angles, and hydrogen bond distances are given in Table 2. The molecular structure with the atoms numbering scheme at 180 K is shown in Figure 1.

The structure consists of a cation $[Fe^{II}H_3L^{Me}]^{2+}$ and the two anions of Cl^- and I_3^-. The Fe^{II} ion assumes an octahedral coordination environment with the N_6 donor atoms of three Fe−N (imine) bonds and three Fe−N (imidazole) bonds. On the basis of the Fe−N bond distances and N−Fe−N bond angles, the spin state can be identified. The Fe−N bond distances at 180 K are distributed in the range of 2.173(4)−2.221(4) Å, whose values are the typical distances expected for the HS Fe^{II} complex with similar N_6 donor atoms. The Fe−N bond distances at 90 K are distributed in the range of 1.994(3)−2.067(3) Å, whose values are the typical distances expected for the LS Fe^{II} complex. The average Fe−N bond length decreases from 2.195 Å at 180 K to 2.022 Å at 90 K by 0.173 Å, whose value is comparable with 0.176 and 0.179 Å reported for $[Fe^{II}H_3L^{Me}][Fe^{II}L^{Me}]PF_6$.[6c] The N−Fe−N bond angle indicates a more regular octahedron geometry in the

(5) (a) Hayami, S.; Gu. Z.: Shiro, M.; Einaga, A. Fujishima, A.; Sato, O. *J. Am. Chem. Soc.* **2000**, *122*, 7126−7127. (b) Hayami, S.; Gu, Z.; Yoshiki, H.; Fujishima, A.; Sato, O. *J. Am. Chem. Soc.* **2001**, *123*, 11644−11650. (c) Boca, R.; Boca, M.; Dihan, L.; Falk, K.; Fuess, H.; Haase, W.; Jarosciak, R.; Papankova, B.; Renz, F.; Vrbova, M.; Werner, R. *Inorg. Chem.* **2001**, *40*, 3025−3033. (d) Zhong, Z. J.; Tao, J.-O.; Yu, Z.; Dun, C.-Y.; Liu, Y.-J.; You, X.-Z. *J. Chem. Soc., Dalton Trans.* **1998**, 327−328. (e) Létard, J.-F.: Guionneau, P.; Codjovi, E.; Lavastre, O.; Bravic, G.; Chasseau, D.; Kahn, O. *J. Am. Chem.* Soc. **1997**, *119*, 10861−10862.

(6) (a) Sunatsuki, Y.; Ikuta, Y.; Matsumoto, N.; Ohta, H.; Kojima, M.; Iijima, S.; Hayami, S.; Maeda, Y.; Kaizaki, S.; Dahan, F.; Tuchagues, J.-P. *Angew. Chem., Int. Ed.* **2003**, *42*, 1614−1618. (b) Ikuta Y.; Ooidemizu, M.; Yamahata, Y.; Yamada, M.; Osa, S.; Matsumoto, N.; Iijima, S.; Sunatsuki, Y.; Kojima, M.; Dahan, F.; Tuchagues, J.-P. *Inorg. Chem.* **2003**, *42*, 7001−7017. (c) Yamada, M.; Ooidemizu, Ikuta, Y.; M.; Osa, S.; Matsumoto, N.; Iijima, S.; Kojima, M.; Dahan, F.; Tuchagues, J.-P. *Inorg. Chem.* **2003**, *42*, 8406−8416. (d) Sunatsuki, Y.; Ohta, H.; Kojima, M.; Ikuta, Y.; Goto, Y.; Matsumoto, N.; Iijima, S.; Akashi, H.; Kaizaki, S.; Dahan, F.; Tuchagues, J. -P. *Inorg. Chem.* **2004**, *43*, 4154−4171.

Table 2. Relevant Coordination Bond Lengths (Å), Angles (deg), and Hydrogen Bond Distances (Å) for $[Fe^{II}H_3L^{Me}]Cl{\cdot}I_3$ (**2**) at 180 and 90 K[a]

param	180 K	90 K
Fe−N(2)	2.187(4)	2.019(3)
Fe−N(3)	2.202(4)	2.067(3)
Fe−N(5)	2.173(4)	2.025(3)
Fe−N(6)	2.221(4)	2.030(3)
Fe−N(8)	2.176(4)	1.997(2)
Fe−N(9)	2.210(4)	1.994(3)
N(2)−Fe−N(3)	77.05(14)	81.30(11)
N(2)−Fe−N(5)	97.04(16)	94.92(12)
N(2)−Fe−N(6)	90.05(15)	87.67(11)
N(2)−Fe−N(8)	100.69(16)	97.92(12)
N(2)−Fe−N(9)	168.93(13)	173.94(11)
N(3)−Fe−N(5)	166.97(14)	172.41(11)
N(3)−Fe−N(6)	91.55(13)	93.08(10)
N(3)−Fe−N(8)	91.74(13)	89.81(10)
N(3)−Fe−N(9)	92.24(14)	93.00(11)
N(5)−Fe−N(6)	76.71(14)	80.14(10)
N(5)−Fe−N(8)	100.82(14)	97.25(9)
N(5)−Fe−N(9)	94.01(16)	90.98(11)
N(6)−Fe−N(8)	169.21(16)	174.04(11)
N(6)−Fe−N(9)	93.05(15)	94.72(12)
N(8)−Fe−N(9)	76.56(15)	79.92(11)
Hydrogen Bonds		
Cl···N(4)*	3.089(4)	3.140(3)
Cl···N(7)**	3.159(4)	3.164(3)
Cl···N(10)	3.102(4)	3.093(3)

[a] Symmetry Operations: (∗), $-x$, $-y$, $1-z$; (∗∗), $-x$, $1/2+y$, $3/2-z$.

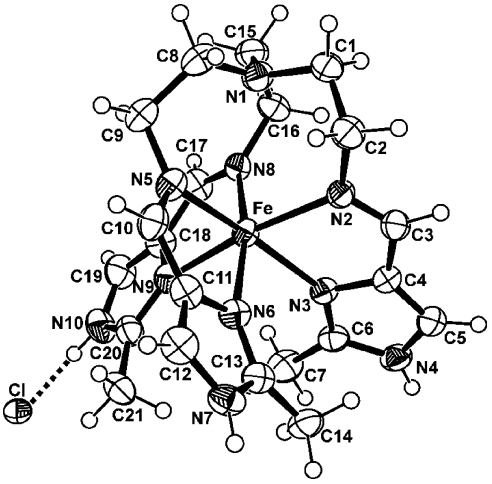

Figure 1. Molecular structure of $[Fe^{II}H_3L^{Me}]Cl{\cdot}I_3$ (**2**) at 180 K with the atom-numbering scheme, where the thermal ellipsoids are drawn with a 50% probability level and the I_3^- ion is omitted.

LS than in the HS state (for example, N(2)−Fe-N(3), 77.05(14)° at 180 K, 81.30(11)° at 90 K).

The extended network structure of **2** is shown in Figure 2a−c. As shown in Figure 2a, the chloride ion plays the role of connector through hydrogen bonds between Cl^- and the imidazole NH groups of three neighboring cations $[Fe^{II}H_3L^{Me}]^{2+}$, while the I_3^- ion exists as an isolated counteranion. One Cl^- ion is hydrogen-bonded to the imidazole NH groups of three adjacent cation $[Fe^{II}H_3L^{Me}]^{2+}$ to produce a 2D layered structure, in which the hydrogen bond distances are Cl···N(4)* = 3.089(4), Cl···N(7)** = 3.159(4), and Cl···N(10) = 3.102(4) Å at 180 K and Cl···N(4)* = 3.140(3), Cl···N(7)** = 3.164(3), and Cl···N(10) = 3.093(3) Å at 90 K. It should be noted that all three imidazole NH groups

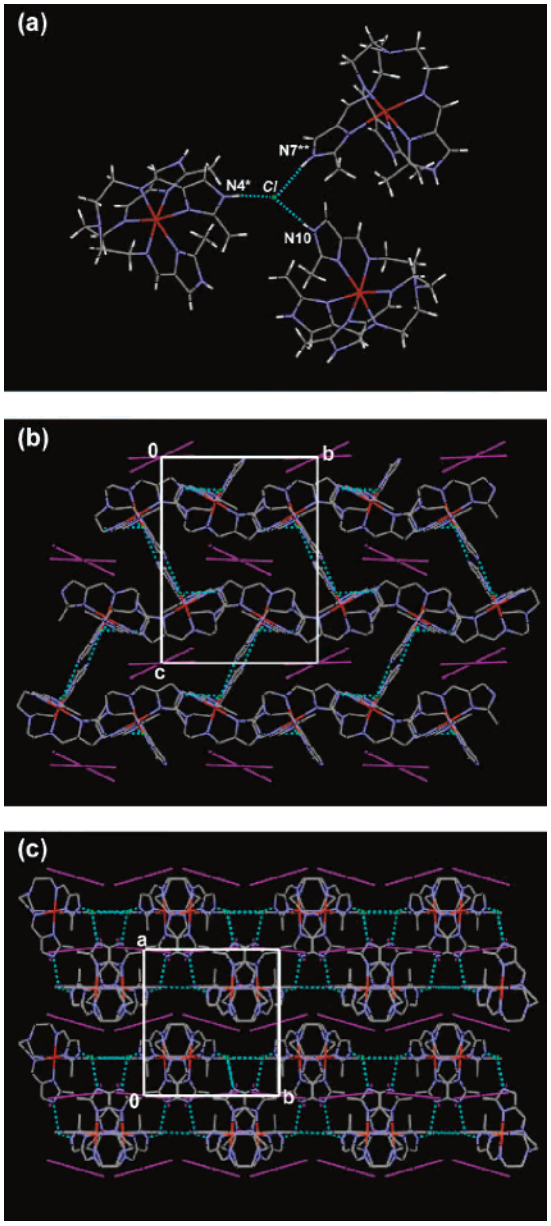

Figure 2. (a) One Cl^- ion hydrogen-bonded to three imidazole NH groups of three adjacent cationic complexes $[Fe^{II}H_3L^{Me}]^{2+}$, in which the hydrogen bond distances at 180 K are Cl···N(4)* = 3.089(4), Cl···N(7)** = 3.159(4), and Cl···N(10) = 3.102(4) Å. The symbols ∗ and ∗∗ denote the symmetry operations of $-x$, $-y$, $1-z$ and $-x$, $y+1/2$, $-z+3/2$, respectively. (b) Top view of a 2D layer. The cations $[Fe^{II}H_3L^{Me}]^{2+}$ and anions Cl^- are hydrogen-bonded to form a 2D layered structure. (c) Side view showing the stacking manner of 2D layers. One of the two unique I_3^- ions is positioned between the 2D layers, and another exists in a cavity of a 2D layer. The I_3^- ion in the cavity is disordered at 180 K but not at 90 K.

of the $[Fe^{II}H_3L^{Me}]^{2+}$ cation participate in the construction of the 2D layer structure. The geometry of ClN_3 defined by the Cl^- ion and three hydrogen-bonded imidazole nitrogen atoms N_3 is not planar, because four paired electrons of the Cl^- ion with the $[Ne](3s)^2(3p)^6$ electronic configuration should be oriented in a tetrahedral geometry due to the sp^3 configuration. As shown in Figure 2c, each 2D layer occupies a thickness corresponding to a two complex-molecule size and the 2D layers are separated by a layer of I_3^- ions. The cation $[Fe^{II}H_3L^{Me}]^{2+}$ is a chiral species with the Δ (clockwise)

or Λ (anticlockwise) configuration due to the screw coordination arrangement of the achiral tripod ligand around the Fe^{II} ion. Within a 2D layer, the Δ and Λ enantiomers coexist, and therefore, the present 2D layer is not a homochiral layer but a racemic layer, whereas the 2D layer of $[Fe^{II}H_3L^{Me}]$-$[Fe^{II}L^{Me}]X$ and $[Co^{III}H_3L^{Me}][Co^{III}L^{Me}]X_3$ constructed by the imidazole−imidazolate hydrogen bonds is a homochiral layer.[6,7]

There are crystallographically two I_3^- ions. One of the two unique I_3^- ions is positioned between the 2D layers, and another exists in a cavity of a 2D layer. At 180 K, the iodine atom I(4) of the I_3^- ion accommodated within a 2D layer was found to be disorderd, and after refinement of the occupancy factors, the two positions were refined in a 50:50 ratio. At 90 K, I(4) has higher thermal parameters than those of the other iodine atoms, but disordered positions could not be separated, demonstrating that the disorder disappeared. The order−disorder problem of the I_3^- ion may be related to the spin crossover, as known for the other SC complexes.[8]

Magnetic Properties of $[Fe^{II}H_3L^{Me}]I_2\cdot H_2O\cdot MeOH$ (1) and $[Fe^{II}H_3L^{Me}]Cl\cdot I_3$ (2). The magnetic susceptibilities of the polycrystalline samples were measured in the temperature range 5−300 K at a slow sweep rate of 1 K min^{-1} under an applied magnetic field of 1 T, in which the sample weight of 20.99 mg was used for **2** and the sample was packed in gelatin capsule with 4 mm of diameter. The sample was quickly cooled to 5 K from room temperature, and the magnetic susceptibility was measured while raising the temperature from 5 to 300 K. Subsequently, the magnetic susceptibility was measured while lowering the temperature from 300 to 5 K. The magnetic behavior of **1** during the warming and cooling modes is very similar. The $\chi_M T$ value/Fe (χ_M is the molar magnetic susceptibility and T the absolute temperature) is practically constant in the overall temperature range at ca. 3.5 cm^3 K mol^{-1}, as expected for HS-Fe^{II} ($S = 2$).

The $\chi_M T$ versus T plots for **2** are shown in Figure 3. The magnetic behavior during the warming and cooling modes is very similar except below 70 K. The difference in magnetic behavior below 70 K can be ascribed to the frozen-in effect. Compound **2** showed no detectable thermal hysteresis in the SC region. The SC behavior in the cooling mode (without frozen-in effect) is described hereafter. In the 300−150 K region, the $\chi_M T$ value is nearly constant at ca. 3.5 cm^3 K mol^{-1}, as expected for the HS-Fe^{II} species ($S = 2$). Upon further cooling, in the 150−70 K region, the $\chi_M T$ value abruptly decreases and then reaches a plateau value of nearly zero below 70 K, expected for LS Fe^{II} species ($S = 0$). The $T_{1/2}$ temperature is estimated to be 110 K.

Mössbauer Spectra of $[Fe^{II}H_3L^{Me}]Cl\cdot I_3$ (2). The temperature dependence of the Mössbauer spectra of complex

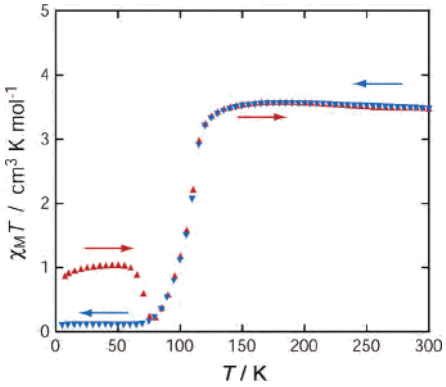

Figure 3. Magnetic behavior of $[Fe^{II}H_3L^{Me}]Cl\cdot I_3$ (**2**) in the form of the $\chi_M T$ versus T plot. The sample was quickly cooled from 300 to 5 K, and the $\chi_M T$ was measured upon elevating the temperature from 5 to 300 K (red triangle) at a rate of 1 K min^{-1}. Subsequently, the $\chi_M T$ was measured upon lowering the temperature from 300 to 5 K (blue triangle). The magnetic difference in the warming and cooling modes below 70 K demonstrates a frozen-in effect.

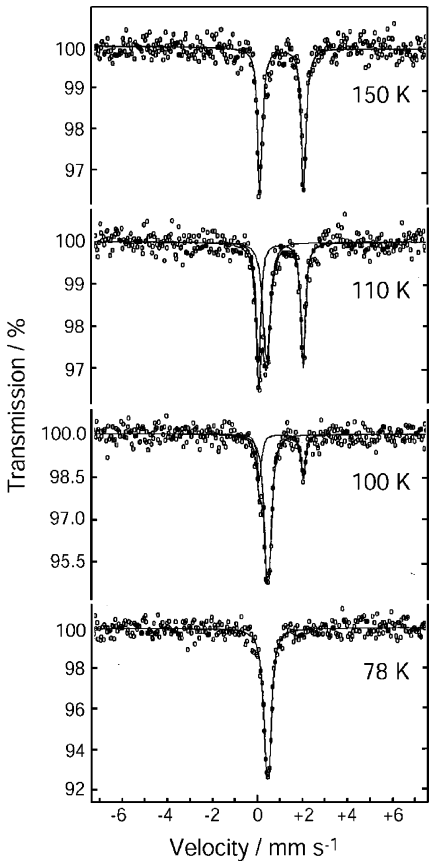

Figure 4. ^{57}Fe Mössbauer spectra of $[Fe^{II}H_3L^{Me}]Cl\cdot I_3$ (**2**) at selected temperatures. The spectra shown were recorded at 150, 110, 100, and 78 K upon warming the sample from 78 K.

2 was investigated, in which the weight and the thickness of the sample are 89.5 mg and 28.5 mg cm^{-2}, respectively. The crystalline sample was packed between aluminum foils and rapidly cooled from room temperature to liquid-nitrogen temperature, 78 K, within 3 min, and the Mössbauer spectra were measured at selected temperatures during the warming mode. Representative spectra are shown in Figure 4. At 78 K, the spectrum consists of a doublet assignable to LS Fe^{II} ($\delta = 0.48$ mm s^{-1} and $\Delta E_Q = 0.15$ mm s^{-1}). For 78−150

(7) (a) Katsuki, I.; Motoda, Y.; Sunatsuki, Y.; Matsumoto, N.; Nakashima, T.; Kojima, M. *J. Am. Chem. Soc.* **2002**, *124*, 629−640. (c) Mimura, M.; Matsuo, T.; Motoda, Y.; Matsumoto, N.; Nakashima, T.; Kojima, M. *Chem. Lett.* **1998**, 691−692. (b) Sunatsuki, Y.; Motoda, Y.; Matsumoto, N. *Coord. Chem. Rev.* **2002**, *226*, 199−209.

(8) (a) Wu, C.-C.; Jung, J.; Gantzel, P. K.; Gütlich, P.; Hendrickson, D. N. *Inorg. Chem.* **1997**, *36*, 5339−5347. (b) Money, V. A.; Elhaik, J.; Evans, B.; Halcrow, M. A.; Howard, J. A. K. *J. Chem. Soc., Dalton Trans.* **2004**, 65−69.

Table 3. Mössbauer Parameters for $[Fe^{II}H_3L^{Me}]Cl{\cdot}I_3$ (**2**)

T/K	δ^a/mm·s^{-1}	ΔE_Q/mm·s^{-1}	rel area/%
298	1.01	1.76	100
200	1.05	1.89	100
150	1.10	1.96	100
120	1.10	2.00	80
	0.44	0.10	20
110	1.11	1.99	58
	0.47	0.13	42
100	1.08	1.95	28
	0.47	0.15	72
90	1.08	1.97	16
	0.47	0.16	84
78	0.48	0.15	100
50	0.48	0.16	100
4.2	0.49	0.16	100

[a] Isomer shift data are referenced to iron foil. [b] The experimental errors for δ and ΔE_Q are less than 0.01 mm·s^{-1}. The molar fractions of HS and LS species contain the experimental error of several percent.

K, the spectra consist of two quadrupole-split doublets assigned to the LS and HS Fe^{II} sites (for example at 110 K LS Fe^{II} (δ = 0.47 mm s^{-1}, ΔE_Q = 0.13 mm s^{-1}) and HS Fe^{II} (δ = 1.11 mm s^{-1}, ΔE_Q = 1.99 mm s^{-1})). In the 298−150 K temperature range, they consist of a doublet assignable to HS Fe^{II} (isomer shift δ = 1.10 mm s^{-1} and quadruple splitting ΔE_Q = 1.96 mm s^{-1} at 150 K). To examine the frozen-in effect, after the above measurements the sample was rapidly cooled from room temperature to 4.2 K within 3 min and the Mössbauer spectra were measured at selected temperatures (4.2 and 50 K) during the warming mode. Below 78 K, the spectra consist of a doublet assignable to LS Fe^{II}, suggesting that there is no frozen-in effect in the Mössbauer spectra, while the magnetic susceptibility measurements could detect the frozen-in effect. This disagreement between the Mössbauer and magnetic susceptibility results can be due to the weak cooperativity discussed later but is not clear at present.

A deconvolution analysis of the spectrum at each temperature was performed to determine the molar fraction of the HS Fe^{II} versus total Fe^{II}. The resulting Mössbauer parameters are listed in Table 3. The plots of the HS Fe^{II} versus total Fe^{II} molar fraction derived from the Mössbauer spectra and the magnetic susceptibility measurements are shown in Figure 5. Except for the frozen-in effect, the Mössbauer data are consistent with the magnetic susceptibility result, both showing an abrupt SC.

LIESST Effects of $[Fe^{II}H_3L^{Me}]Cl{\cdot}I_3$ (2). Light irradiations with various wavelengths at 5 K afford an increase of the $\chi_M T$ value to reach the saturated values depending on the maximum wavelength, where light of various wavelengths (400, 450, 500, 550, 600, 650, 700 nm) passed through an interference filter with an 80 nm fwhm and the diode laser light (806 nm) irradiated the polycrystalline sample. The sample was placed at the edge of the optical fiber, where the power of the light is 2 mW cm^{-2}. The increase in the $\chi_M T$ value is attributed to the spin transition from the LS to HS state due to the light irradiation, that is, the so-called LIESST effect.[2] Among the lights with various wavelengths, the 600 nm light is the most effective to increase the $\chi_M T$ value. As shown in Figure 6, the photoexcitation is almost complete. The saturated $\chi_M T$ value of ca. 2.5 cm^3 K mol^{-1}

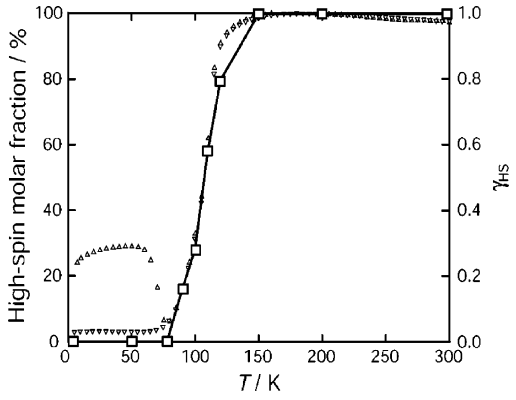

Figure 5. HS Fe^{II} versus total Fe^{II} molar fraction obtained by deconvolution analysis of each Mössbauer spectrum (open squares), together with the HS Fe^{II} versus total Fe^{II} molar fraction obtained from magnetic susceptibility measurements (open triangles). For the Mössbauer spectroscopy, the values were recorded upon warming the sample. The HS fraction γ_{HS} from magnetic susceptibility was calculated using the equation $(\chi_M T)_{obs} = \gamma_{HS}(\chi_M T)_{HS} + (1 - \gamma_{HS})(\chi_M T)_{LS}$, with the limiting values $(\chi_M T)_{HS}$ = 3.5 cm^3 K mol^{-1} and $(\chi_M T)_{LS}$ = 0.0 cm^3 K mol^{-1}.

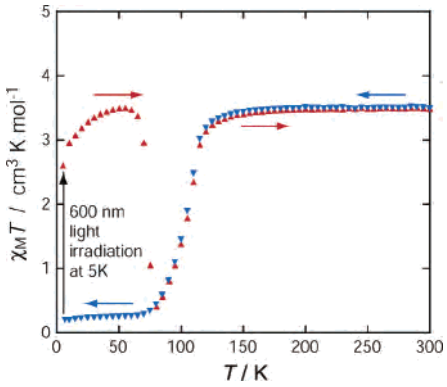

Figure 6. LIEEST effect of $[Fe^{II}H_3L^{Me}]Cl{\cdot}I_3$ (**2**). Light irradiation with maximum wavelength of 600 nm at 5 K afforded an increase of the $\chi_M T$ value. After the light irradiation (600 nm) was switched off, the thermal relaxation process was recorded in the warming mode (red triangles) and then the $\chi_M T$ value from 300 to 5 K in the cooling mode (blue triangles) was measured.

at 5 K is smaller than the expected value of HS Fe^{II}, due to the zero field splitting effect. After the light was switched off, the thermal relaxation was studied. Upon elevation of the temperature, the $\chi_M T$ value increases and reaches the maximum value of ca. 3.5 cm^3 K mol^{-1} at 50 K and then abruptly decreases around 70 K. The $\chi_M T$ increase is most probably due to the zero-field splitting of the S = 2 ground state of the trapped HS Fe^{II} molecules. The maximum value of ca. 3.5 cm^3 K mol^{-1} at 50 K suggests that the Fe^{II} site completely converts from the LS to HS state due to the LIESST effect. The limit LIESST temperature, T(LIESST), which was evaluated from the first derivative of $\chi_M T$ in the HS → LS relaxation after LIESST, is 73 K, where it should be noted that the value is evaluated from the data with 1.0 K min^{-1} sweeping mode.

Recently, Létard et al. examined the correlation between T(LIESST) and $T_{1/2}$ values for a large series of SC compounds and found that these complexes are on the straight lines of general equation $T(\text{LIESST}) = T_0 - 0.3T_{1/2}$ with T_0 = 100, 120, or 150.[9] They proposed that cooperativity stabilizes the photoinduced HS state: the higher the coop-

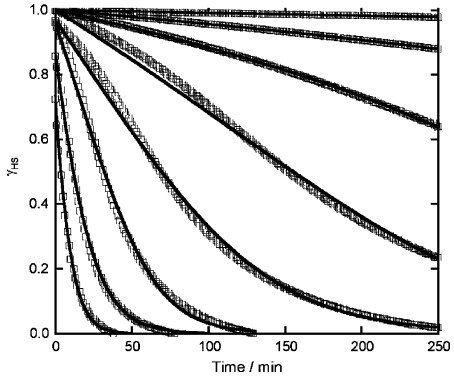

Figure 7. Time dependence at various temperatures of the HS molar fraction, γ_{HS}, generated by the LIESST effect. Solid lines represent the best fit to the experimental HS → LS relaxation curves at different temperatures of 50, 55, 57.5, 60, 62.5, 65, 67.5, and 70 K.

erativity, the higher the T_0 value.[10] The plot of $[Fe^{II}H_3L^{Me}]$-$Cl\cdot I_3$ with T(LIESST) = 73 K and $T_{1/2}$ = 113 K is on the line of the family with T_0 = 100 K, suggesting a weak cooperativity. Other parameters seem to tune the metastable HS state; the T(LIESST) value shows a linear correlation with the distortion of the metal coordination sphere: strong distortions provide more stable photoinduced HS state.[11] As a consequence, increasing overcrowding of the ligand, from a mono- to bi-, tri-, tetra-, and hexadentate ligand, should lead to higher T(LIESST) value. However, in the case of the $[Fe^{II}H_3L^{Me}]Cl\cdot I_3$ complex with a hexadentate ligand, the tripodal hexadentate ligand does not allow a large distortion so that the low value of T(LIESST) can be explained.

HS → LS Relaxation. The temperature dependence of the HS → LS relaxation for $[Fe^{II}H_3L^{Me}]Cl\cdot I_3$ (**2**) has been investigated in the range 20−70 K and is shown in Figure 7, in which the HS molar fraction, γ_{HS}, versus time is plotted at various temperatures. Below 50 K, the HS → LS relaxation is very slow and the relaxation curve can be well fitted by a single-exponential equation. In contrast, for temperatures higher than 55 K, the dynamics of the HS → LS relaxation is faster and the relaxation curves show a sigmoid behavior, suggesting that the HS → LS relaxation is not just for an isolated molecule and there must be some cooperative effects. Previous studies of the HS → LS relaxation kinetics in other $Fe^{II}N_6$ spin-crossover systems have shown similar sigmoid curves.[12] Such a behavior can be interpreted as a self-acceleration of the HS → LS relaxation as γ_{HS} decreases. It has been shown that the self-acceleration is due to the buildup of an internal pressure, or "lattice pressure", caused by the large reduction in size of the spin crossover complex as it converts from HS to LS.[12j]

The relaxation curves can be described by the decay differential eq 1 in which the rate constant for the HS → LS conversion, k_{HL}, depends on the HS fraction through eq 2. E_a* is an additional activation energy due to cooperativity while $k_{HL}(T)$ is the relaxation rate constant at a given temperature. At sufficiently high temperatures $k_{HL}(T)$ is expected to follow an Arrhenius-like eq 3, where E_a is the activation energy associated with the HS → LS relaxation and $k_{HL}{}^0$ the preexponential factor.

$$d\gamma_{HS}/dt = -k_{HL}(\gamma_{HS},T)\gamma_{HS} \quad (1)$$

$$k_{HL}(\gamma_{HS},T) = k_{HL}(T)\exp(-\gamma_{HS}E_a^*/k_BT) \quad (2)$$

$$k_{HL}(T) = k_{HL}{}^0\exp(-E_a/k_BT) \quad (3)$$

At low temperatures, the HS → LS relaxation is very slow and the high spin fraction does not sizable decrease during the considered relaxation time. Therefore, the modification of the internal pressure in that temperature range is negligible and the relaxation can be described by a single exponential as expressed by eq 4.

$$\gamma_{HS}(t) = \exp[-k_{HL}(T)t] \quad (4)$$

Therefore, in the 20−50 K temperature range, the HS → LS relaxation curves can be reasonably well fitted by such a single exponential and the $k_{HL}(T)$ values obtained from a least-squares fitting of the experimental data are listed in Table 4. At temperatures higher than 50 K, the HS → LS relaxation after LIESST is fast and eqs 1 and 2 were utilized to analyze the corresponding sigmoid behavior. These differential equations were numerically integrated through a fourth order Runge−Kutta algorithm, and the least-squares

Table 4. Least-Squares Fitting Parameters for Rate Constants $k_{HL}(T)$ (s^{-1}) and Additional Activation Energies E_a* (cm^{-1}) at Various Temperatures

T/K	$k_{HL}(T)/s^{-1}$	E_a^*/cm^{-1}
20	5.64×10^{-8}	
30	4.44×10^{-8}	
40	1.68×10^{-7}	
50	1.46×10^{-6}	
55	2.57×10^{-5}	46.3
57.5	1.17×10^{-4}	69.6
60	2.36×10^{-4}	71.4
62.5	3.70×10^{-4}	52.5
65	7.93×10^{-4}	47.2
67.5	1.20×10^{-3}	32.1
70	2.25×10^{-3}	24.6

(9) (a) Létard, J.-F.; Capes, L.; Chastanet, G.; Moliner, N.; Létard, S.; Real, J. A.; Kahn, O. *Chem. Phys.* Lett. **1999**, *313*, 115−120. (b) Marcen, M.; Lecren, L.; Capes, L.; Goodwin, H. A.; Létard, J.-F. *Chem. Phys. Lett*. **2002**, *358*, 87−95.

(10) Capes, L.; Létard, J.-F.; Kahn, O. *Chem.*—Eur. J. **2000**, *6*, 2246−2255.

(11) Marchivie, M.; Guionneau, P.; Létard, J.-F.; Chasseau, D. *Acta Crystallogr., Sect. B* **2005**, *61*, 25−28.

(12) (a) Létard, J.-F.; Guionneau, P.; Rabardel, L.; Howard, J. A. K.; Goeta, A. E.; Chasseau, D.; Kahn, O. *Inorg.* Chem. **1998**, *37*, 4432−4441. (b) Hauser, A.; Gütlich, P.; Spiering, H. *Inorg. Chem.* **1986**, *25*, 4245−4248. (c) Capes, L.; Létard, J.-F.; Kahn, O. *Chem. Eur. J.* **2000**, *6*, 2246−2255. (d) Moliner, N.; Salmon, L.; Capes, L.; Muñoz, M. C.; Létard, J.-F.; Bousseksou, A.; Tuchagues, J.-P.; McGarvey, J. J.; Dennis, A. C.; Castro, M.; Burriel, R.; Real, J. A. *J. Phys. Chem. B* **2002**, *106*, 4276−4283. (e) Buchen, T.; Toftlund, H.; Gütlich, P. *Chem.*—Eur. J. **1996**, *2*, 1129−1133. (f) Hinek, R.; Spiering, H.; Schollmeyer, D. Gütlich, P.; Hauser, A. *Chem.*—Eur. J. **1996**, *2*, 1427−1434. (g) Jeftic, J.; Hinek, R.; Capelli, S. C.; Hauser, A. *Inorg. Chem.* **1997**, *36*, 3080−3087. (h) Al-Obaidi, A. H. R.; Jensen, K. B.; McGarvey, J. J.; Toftlund, H.; Jensen, B.; Bell, S. E. J.; Carroll, J. G. *Inorg. Chem.* **1996**, *35*, 5055−5060. (i) Niel, V.; Munoz, M. C.; Gaspar, A. B.; Galet, A.; Levechenko, G.; Real, J. A. *Chem.*—Eur. J. **2002**, *8*, 2446−2453. (j) Hauser, A.; Feftic, J.; Romstedt, H.; Hinek, R.; Spiering, H. *Coord. Chem. Rev.* **1999**, *190*−*192*, 471−491. (k) Enachescu, C.; Constant-Machado, H.; Codjovi, E.; Linares, J.; Boukheddaden, K.; Varret, F. *J. Phys. Chem. Solids* **2001**, *62*, 1409−1422.

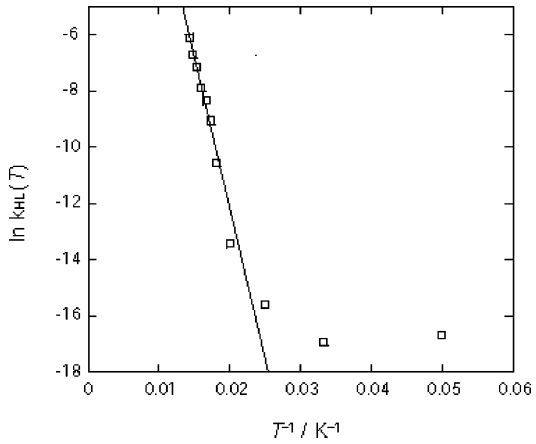

Figure 8. Plots of ln $k_{HL}(T)$ versus $1/T$, where the numerical data are given in Table 4. For the temperature region of $T > 55$ K, a straight line (ln $k_{HL}(T) = 9.27-1071(1/T)$) is obtained. For the temperature region of $T < 50$ K, $k_{HL}(T)$ is almost temperature independent with an average value $k_{HL}(T \rightarrow 0)$ of 5.0×10^{-8} s^{-1}.

fitting of the experimental data to the numerical solutions leads to the $k_{HL}(T)$ and E_a* values reported in Table 4.

The estimated values of E_a* are reasonably constant in the considered range of temperatures with significant deviations only for the two highest temperatures, probably due to the decay which occurs in the warming stage prior to the relaxation measurements as suggested by the initial values at these two temperatures of the HS fraction, respectively 0.87 and 0.74. The mean additional activation energy, E_a*, 57 cm^{-1}, can be compared with the reported values, such as 60, 70, 118, and 164 cm^{-1} for $[Fe^{II}(bptn)_2(NCS)_2]$ (bptn = 1,7-bis(2-pyridyl)-2,6-diazaheptane),[12e] $[Fe^{II}(PM\text{-}FlA)_2(NCS)_2]$ (PM-FlA = *N*-2′-pyridylmethylene-4-(2-amino)fluorene),[12c] $[Fe^{II}(PM\text{-}BiA)_2(NCS)_2]$ (PM-BiA = *N*-2-pyridylmethylene-4-aminobiphenyl),[12a] and $[Fe^{II}(ptz)_6(BF_4)_2]$ (ptz = 1-propyltetrazole), respectively,[12b] indicting that the present complex shows weak cooperativity.

Figure 8 presents the ln $k_{HL}(T)$ versus $1/T$ plot. The plot reveals a nearly temperature-independent relaxation behavior at low temperatures and a thermally activated relaxation behavior at high temperatures. In the temperature region higher than 55 K, the straight line (ln $k_{HL}(T) = 9.27 - 1071(1/T)$) reveals a thermally activated relaxation behavior with $k_{HL}{}^0 = 1.06 \times 10^4$ s^{-1} and $E_a = 744$ cm^{-1}. In the whole investigated temperature region both thermally activated and tunneling deactivation mechanisms play important roles, which cannot be decoupled so that the kinetic parameters deduced from the Arrhenius law, preexponential factor and activation energy, should be considered as apparent values. In the temperature region lower than 40 K, $k_{HL}(T)$ is very small and almost temperature independent with an average ln[$k_{HL}(T \rightarrow 0)$] value of -16.8 ($k_{HL}(T \rightarrow 0) = 5.0 \times 10^{-8}$ s^{-1}), indicating that a pure tunneling mechanism is predominant. This value is quite small compared to other literature data but close to the values observed for Fe^{II} complexes showing weak cooperativity such as $[Fe(PM\text{-}FlA)_2(NCS)_2]$[12c] However, since the high-spin fraction does not sizable decrease during the considered relaxation time, this value is subjected to a significant error and should be taken with care.

In the theory of nonadiabatic multiphonon relaxation,[13a] the low-temperature tunneling rate constant for the HS $\rightarrow$ LS relaxation $k_{HL}{}^0$ is given by $k_{HL}(T \rightarrow 0) = (2\pi/\hbar^2\omega)(\beta_{HL})^2\Omega_{LS}$-$(S^p e^{-S}/p!)$, where $\beta_{HL} = \langle\Phi_{HS}|H_{SO}|\Phi_{LS}\rangle$ is the electronic matrix element of the spin−orbit coupling between the HS and LS states, $\hbar\omega$ is the frequency of the breathing vibration of the $Fe^{II}N_6$ core, and $\Omega_{LS} = 1$ is the electronic degeneracy of the final LS state. $S = 1/2f(\Delta Q_{HL}{}^2/\hbar\omega)$ is the Huang−Rhys factor, which is a measure of the horizontal displacement of the HS and LS wells, ΔQ_{HL} being the reduced coordinate change ($\Delta Q_{HL} = \sqrt{6}\Delta r_{HL}$) and f the force constant for the Fe−N bond. The parameter $p = \Delta E^0{}_{HL}/\hbar\omega$ is the reduced energy gap between the two wells.

A correlation between ln[$k_{HL}(T \rightarrow 0)$] and $T_{1/2}$ has been observed by Hauser et al.[13b] for a series of $Fe^{II}N_6$ SC compounds, showing an increase of $k_{HL}(T \rightarrow 0)$ as $T_{1/2}$ increases. For $[Fe^{II}H_3L^{Me}]Cl{\cdot}I_3$, $T_{1/2} = 113$ K and the calculated $k_{HL}(T \rightarrow 0)$, 5.0×10^{-8} s^{-1}, basically follows this correlation, being only slightly lower than expected on the basis of a Huang−Rhys factor $S \approx 50$ obtained from the theoretical fit of the literature values for a series of $Fe^{II}N_6$ SC compounds.[13b]

Experimental Section

Materials. All chemicals and solvents were reagent grade and were obtained from Tokyo Kasei Co., Ltd., and Wako Pure Chemical Industries, Ltd. They were used for the synthesis without further purification.

$[Fe^{II}H_3L^{Me}]I_2{\cdot}H_2O{\cdot}$MeOH (1). Tris(2-aminoethyl)amine (0.75 g, 5 mmol) was added to a solution of 2-methyl-4-formylimidazole (1.65 g, 15 mmol) in 20 mL of methanol, and the mixture was stirred at 50 °C for 10 min. The methanolic solution of the tripod ligand thus prepared was used without isolation of the ligand for the synthesis of the metal complexes. To the tripod ligand solution (5 mmol) was added a solution of $Fe^{II}Cl_2{\cdot}4H_2O$ (0.994 g, 5 mmol) in 20 mL of methanol and then a solution of NaI (1.51 g, 10 mmol) in 20 mL of methanol. The mixture was stirred for several hours and then filtered. The filtrate was allowed to stand for several days, during which time the precipitated yellow crystals were collected by suction filtration, washed with a small volume of methanol, and dried in vacuo. Recrystallization was performed from the methanol solution containing a small amount of ascorbic acid at ambient temperature. Anal. Calcd for $[Fe^{II}H_3L^{Me}]I_2{\cdot}H_2O{\cdot}$MeOH: C, 33.77; H, 4.63; N, 17.90. Found: C, 34.02; H, 4.32; N, 18.16. IR (KBr): $\nu_{C=N}$ 1640 cm^{-1}.

$[Fe^{II}H_3L^{Me}]Cl{\cdot}I_3$ (2). Method A. To the tripodal ligand solution (5 mmol in 10 mL of methanol) was added a solution of $Fe^{II}Cl_2{\cdot}4H_2O$ (0.994 g, 5 mmol) in 20 mL of methanol and then a solution of NaI (2.265 g, 15 mmol) in 20 mL of methanol. To the solution was added a small amount of aqueous HCl solution to adjust the pH 5. The mixture was stirred for 5 min at ambient temperature and then filtered. The filtrate was allowed to stand for several days, during which time compound **1** and **2** crystals precipitated.

Method B. To the tripod ligand solution (5 mmol) was added a solution of $Fe^{III}Cl_3$ (0.81 g, 5 mmol) in 20 mL of methanol and then a solution of NaI (2.30 g, 15 mmol) in 20 mL of methanol. The mixture was stirred for 1 day at 30 °C and then filtered. The

(13) (a) Buhks, E.; Navon, G.; Bixon, M.; Jortner, J. *J. Am. Chem. Soc.* **1980**, *102*, 2918−2923. (b) Hauser, A. *Coord. Chem. Rev.* **1991**, *111*, 273−290.

filtrate was allowed to stand for several days during which time red crystals precipitated. They were collected by suction filtration, washed with a small volume of methanol, and dried in vacuo. Recrystallization was performed from the methanol solution. Anal. Calcd for $[Fe^{II}H_3L^{Me}]Cl\cdot I_3$: C, 28.20; H, 3.38; N, 15.66. Found: C, 28.06; H, 3.27; N, 15.33. IR (KBr): $\nu_{C=N}$ 1644 cm^{-1}.

Physical Measurements. Elemental C, H, and N analyses were carried out by Kikue Nishiyama at the Center for Instrumental Analysis of Kumamoto University. Infrared spectra were recorded on a Perkin-Elmer FT-IR PARAGON 1000 spectrometer using KBr disks at ambient temperature. The magnetic susceptibilities were measured using a MPMS5 SQUID (Quantum Design) in the 5−300 K temperature range at the 1 K min^{-1} sweeping mode under an applied magnetic field of 1 T. The calibration was done with palladium metal. Corrections for diamagnetism were applied using Pascal's constants.[14] For the LIESST experiment, a xenon arc lamp (Hamamatsu L7810) and diode laser (806 nm, ILX Lightwave LDT-5525, LDX-3525) were used as the light sources. The interference filtered light of a xenon arc lamp was guided via an optical fiber into the SQUID magnetometer. The sample was placed on the edge of the optical fiber. The measurements were performed on a very thin layer of the powder sample. The weight was estimated by comparing the thermal spin crossover curve with that for a heavier and accurately weighed sample. The Mössbauer spectra were recorded using a Wissel 1200 spectrometer and a proportional counter. As the radioactive source, ^{57}Co(Rh) moving in a constant acceleration mode was used. The hyperfine parameters were obtained by least-squares fitting to Lorentzian peaks. The isomer shifts are reported relative to metallic iron foil. The sample temperature was controlled by a Heli-tran liquid transfer refrigerator (Air Products and Chemicals, Inc.) with an accuracy of ±0.5 K.

Crystallographic Data Collection and Structure Determination for $[Fe^{II}H_3L^{Me}]Cl\cdot I_3$ (2) at 180 and 90 K. A red block crystal of 0.40 × 0.30 × 0.10 mm^3 was mounted on a Stoe imaging plate diffractometer system (IPDS) equipped with an Oxford Cryosystems cooler device using graphite-monochromated Mo Kα radiation (λ = 0.710 73 Å). The crystal-to-detector distance was 70 mm ($2\theta_{max}$ value 52.1°). Data were collected at 180 K with a φ oscillation movement (φ = 0.0−200.2°, $\Delta\varphi$ = 1.4°).[15] A total of 24 770 reflections were found of which 6112 independent (R_{int} = 0.0444) ones were collected. Numerical absorption corrections were applied for $T_{min-max}$ = 0.2914−0.6983.[16] The crystal was then slowly warmed to room temperature, transferred to an Oxford-Diffraction Xcalibur diffractometer, and cooled to 50 K with an Oxford Instruments Helijet cooler device, but it lost crystallinity by the end of the cooling process. A new crystal (red block, 0.30 × 0.25 × 0.15 mm^3) was then mounted on an Oxford-Diffraction Xcalibur diffractometer using graphite-monochromated Mo Kα radiation (λ = 0.710 73 Å) and equipped with an Oxford Instruments Cryojet cooler device. Data were collected[17] at 90 K with 4 runs (ϕ = 0, 90, 180, 270°) and ω scans up to θ = 32.0° (143 frames with a maximum time of 15 s). As the crystallinity disappeared during the data collection, only the 2 complete first runs and the 40 first frames of the third run were used. Fortunately, after the unit-cell determination, a crystal movie was made before the data collection. So, Gaussian absorption corrections could be applied ($T_{min-max}$ = 0.3453−0.5757). A total of 16 357 reflections (from 28 526 collected) were used, of which 8082 were independent (from the 10 004 expected) (R_{int} = 0.0388).[18]

The structures were solved using SHELXS-97[19] and refined on F^2 by full-matrix least squares using SHELXL-97[20] with anisotropic displacement parameters for all non-hydrogen atoms. As structures were solved with the pertinent geometry, refinement did not converge. It could be suspected that monoclinic with β angle nearly equal to 90° may emulate orthorhombic symmetry. A twin instruction (100 0$\bar{1}$0 00$\bar{1}$) was introduced. The parameter for unequal components converged to 0.46 at 180 K and to 0.26 at 90 K. Refinement was achieved with H atoms introduced in calculations using the riding model. Isotropic U_H were 1.1 times higher than those of the atom to which they are bonded. At 180 K, the iodine atom I(4) was found disordered, and after refinement of occupancy factors, the two positions were refined in the 50/50 ratio. At 90 K, atom I(4) has higher thermal parameters than those of the other iodine atoms, but the disordered positions could not be separated. The atomic scattering factors and anomalous dispersion terms were taken from the standard compilation.[21] The maximum and minimum peaks on the final difference Fourier map were 0.89 and −1.09 e $Å^{-3}$ at 180 K and 1.03 and −0.89 e $Å^{-3}$ at 90 K. Crystal data collection and refinement parameters are given in Table 1.

Acknowledgment. This work was supported in part by a Grant-in-Aid for Science Research (No. 16205010 and No. 17350028) from the Ministry of Education, Science, Sports, and Culture of Japan. N.B. was supported by JSPS program for foreign postdoctoral research fellow (No. P04806).

Supporting Information Available: X-ray crystallographic files in CIF format for compounds **2**. This material is available free of charge via the Internet at http://pubs.acs.org. See http://www.rcs.org/suppdata/dt/ for crystallographic data in CIF or other electronic format.

IC050008F

(14) Kahn, O. *Molecular Magnetism*; VCH: Weinheim, Germany, 1993.
(15) *STOE, IPDS Manual*, version 2.93; Stoe & Cie: Darmstadt, Germany, 1997.
(16) *Stoe, X-SHAPE. Crystal Optimisation for Numerical Absorption Corrections*, revision 1.01; Stoe & Cie: Darmstadt, Germany, 1996.
(17) Watkin, D. J.; Prout, C. K.; Carruthers, J. R.; Betteridge, P. W. *CRYSTALS Issue 11*, 1996; Chemical Crystallography Laboratory: Oxford, U.K. *CRYSALIS*, version 170; Oxford-Diffraction: Oxford, U.K., 2002.
(18) Spek, A. L. PLATON. An Integrated Tool for the Analysis of the Results of a Single-Crystal Structure Determination. *Acta Crystallogr., Sect. A* **1990**, *A46*, C34.
(19) Sheldrick, G. M. *SHELXS-97. Program for Crystal Structure Solution*; University of Göttingen: Göttingen, Germany, 1990.
(20) Sheldrick, G. M. *SHELXL-97. Program for the refinement of crystal structures from diffraction data*; University of Göttingen: Göttingen, Germany, 1997.
(21) *International Tables for Crystallography*; Kluwer Academic Publishers: Dordrecht, The Netherlands, 1992; Vol. C.